Investigation of a four-way coupling regime using a corrected point-particle approach

By M. Esmaily AND J. Horwitz

1. Motivation and objectives

Accurate numerical prediction of particle-particle collisions in particle-laden flows is of concern in various applications. One example concerns modeling the formation of a cloud, which requires accurate prediction of the coalescence of small droplets. In computational models designed for this purpose, droplets are treated as particles and coalescence as the collision between particles, thus emphasizing the need for accurate prediction of particle-particle collisions (Sundaram & Collins 1997).

Collision dynamics between particle pairs whose size are small relative to the unladen fluid scales can be thought to be governed by a superposition of far- and near-field dynamics. At large separations compared to the particle size, particle relative motion is not largely affected by the mutual disturbance fields of the particle pair. In the far field, the relative velocity should be well characterized by the turbulence intensity and Stokes number. However, when particle pairs move at separations comparable to their size, each particle experiences a disturbance flow created by the other, which can change its trajectory. This change manifests as a modification to the drag that can be estimated assuming a locally Stokesian flow on the scale of the particles. For example, a pair of settling particles at a fixed separation comparable to their size can experience drag reductions exceeding 30% of what each would experience in isolation (Stimson & Jeffrey 1926; Batchelor 1972). In addition, the variation in separation distance of colliding particles makes the drag dependence more complicated (Ardekani & Rangel 2006; Sundararajakumar & Koch 1996). These observations suggest that mutual disturbances at small separations can have a significant effect on modifying particle trajectories. Therefore, incorporating models of the mutual disturbance into a numerical simulation would likely increase the accuracy of the prediction of particle near-field statistics and collision frequency.

Various methods with different levels of fidelity can be used for numerical simulations of flows laden with small particles. On one end of the spectrum, there is the Eulerian-Eulerian technique with no notion of individual particles, hindering its *a-posteriori* predictive capability when particle-particle interactions are concerned. On the other end of the spectrum, there is the particle-resolved method that can accurately resolve the disturbance field near particles. Its shortcoming, however, is its prohibitive computational cost, particularly in scenarios involving a large number of particles. Here, we focus on a method in the middle of this spectrum, namely the Eulerian-Lagrangian technique, which has a reasonable cost and accuracy. Within the Eulerian-Lagrangian category, there are multiple levels of fidelity categorized by how particles influence the flow. When inertial particles experience a hydrodynamic force but the flow does not experience the opposite force, the system is said to be one-way coupled; when the opposite of the drag force is applied to the fluid, the system is two-way coupled. An additional distinction in the two-way coupling regime can be identified when the two-way coupling force is applied

in a consistent manner called corrected two-way coupled. The latter method refers to a scheme in which the disturbance created by each particle is taken into account when computing the force that each particle experiences (Esmaily & Horwitz 2017; Horwitz & Mani 2016; Ireland & Desjardins 2017). Such a correction can become important since the force (Stokes drag or otherwise), which is formulated on the basis of the undisturbed fluid velocity, can be calculated incorrectly if the fluid velocity at the location of the particle is used as an estimation of the undisturbed fluid velocity. In our earlier work, we proposed a correction scheme that not only provides an accurate estimate of the drag on a single particle; it can also capture the change in the drag due to the influence of a nearby particle by partly resolving the near-field disturbances (Esmaily & Horwitz 2017). In this study, we are interested in investigating how this correction scheme changes the prediction of collision and clustering statistics in a four-way coupling regime where particles can collide in addition to experiencing hydrodynamic interactions with the carrier fluid.

For this purpose, we investigate a decaying particle-laden homogeneous isotropic turbulent flow at relatively high loading. In what follows, a short overview of the correction scheme is provided and followed by a discussion of the problem setup and data acquisition procedure. Finally, we draw conclusions and discuss future directions.

2. A correction method for point-particle simulations

The full description of the correction procedure, which is discussed here to a limited extent, is provided by Esmaily & Horwitz (2017). Specifically, treatment of anisotropic grids and step-by-step derivation of the correction method are eliminated from this report for the sake of brevity. The extent to which details are provided is to ensure that the results reported in Section 3 can be reproduced independently. In what follows, we use Roman subscripts, italic subscripts, and italic superscripts in parentheses to denote various parameters, computational grid points, and directions of the Cartesian coordinate system, respectively.

Newton's second law expresses the motion of a particle as

$$m_{\mathrm{p}}\dot{\boldsymbol{u}}_{\mathrm{p}} = \boldsymbol{F}, \tag{2.1}$$

where m_p is the mass of the particle, $\boldsymbol{u}_{\mathrm{p}}$ is the particle velocity, $\dot{(\bullet)}$ denotes the Lagrangian time derivative and $\boldsymbol{F}$ is the two-way coupling (drag) force that is exerted from the flow on the particle. We model $\boldsymbol{F}$ using a quasi-steady drag law

$$\boldsymbol{F} = 3\pi\mu d_{\mathrm{p}} C_{\mathrm{r}}(\mathrm{Re}_{\mathrm{p}})(\boldsymbol{u}_{\mathrm{f}} - \boldsymbol{u}_{\mathrm{p}}), \tag{2.2}$$

where d_{p} is the particle diameter, μ is the fluid dynamic viscosity, $C_{\mathrm{r}}(\mathrm{Re}_{\mathrm{p}})$ is a correction factor for finite Reynolds number effects, Re_{p} is the particle Reynolds number, and $\boldsymbol{u}_{\mathrm{f}}$ is the undisturbed fluid velocity at the location of particle. The correction to the Stokes drag is obtained from an empirical relationship by Clift *et al.* (2005); i.e.,

$$C_{\mathrm{r}}(\mathrm{Re}) = 1 + 0.15\mathrm{Re}^{0.687}. \tag{2.3}$$

The particle Reynolds number is also defined based on the particle slip velocity as

$$\mathrm{Re}_{\mathrm{p}} = \frac{\|\boldsymbol{u}_{\mathrm{f}} - \boldsymbol{u}_{\mathrm{p}}\| d_{\mathrm{p}}}{\nu}, \tag{2.4}$$

where $\nu = \mu/\rho_{\mathrm{f}}$ is the kinematic viscosity of the fluid. Depending on the regime under

consideration, other terms can appear in Eq. (2.2) to model buoyancy, added mass, lift, and history effects. These additional terms can be included as needed since the following correction scheme is designed for a generic $\boldsymbol{F}$. However, we have chosen to neglect these other forces in this particular study. In a two-way coupling regime, the opposite of $\boldsymbol{F}$ is applied to the fluid, which is governed by

$$\frac{\partial \boldsymbol{u}}{\partial t} + \boldsymbol{u} \cdot \nabla \boldsymbol{u} = \frac{1}{\rho_{\mathrm{f}}} \nabla \cdot \boldsymbol{T} - \sum_{i=1}^{N_{\mathrm{p}}} \frac{\boldsymbol{F}_i}{m_{\mathrm{c}}} \delta_a(\boldsymbol{x} - \boldsymbol{x}_{\mathrm{p},i}), \tag{2.5}$$

where $\boldsymbol{u}(\boldsymbol{x}, t)$ is the Eulerian representation of fluid velocity, $\boldsymbol{T}$ is the stress tensor, N_{p} is the number of particles, $\boldsymbol{F}_i$ is the two-coupling force associated with the i^{th} particle, $m_{\mathrm{c}} = \rho_{\mathrm{f}} a^3$ is the mass of the fluid in the computational cell that has a size $a \times a \times a$, δ_a is the Dirac delta function that distribute the force over the cell volume via trilinear interpolation and $\boldsymbol{x}_{\mathrm{p},i}$ is the position of i^{th} particle.

It is critical to observe that the computation of $\boldsymbol{F}$ in Eq. (2.2) depends on the knowledge of the undisturbed fluid velocity $\boldsymbol{u}_{\mathrm{f}}$. The undisturbed velocity is the fluid velocity when the flow is not altered or disturbed by the particle. In a continuous setting, the velocity of the fluid in the neighborhood of the particle is certainly affected by the particle and is not a good candidate for the undisturbed velocity. Nevertheless, in the point-particle simulation framework that same near-particle velocity is often adopted as an estimate of the undisturbed velocity. In two-way coupled simulations, the fluid velocity interpolated at the location of the particle (denoted by the disturbed fluid velocity $\boldsymbol{u}_{\mathrm{d}}$) does not necessarily provide an accurate estimate of the undisturbed fluid velocity, as the value of the latter is modified (disturbed) by the presence of the particle. The difference between $\boldsymbol{u}_{\mathrm{f}}$ and $\boldsymbol{u}_{\mathrm{d}}$ can translate into a significant error in the prediction of the settling velocity of a particle under gravity (Figure 1). A similar observation has been made in particle-laden turbulent flows. A comparison against particle-resolved simulations has shown that a naive adoption of the disturbed velocity $\boldsymbol{u}_{\mathrm{d}}$ as a substitute for the undisturbed velocity $\boldsymbol{u}_{\mathrm{f}}$ produces inaccurate particle and fluid statistics (Subramaniam *et al.* 2014). The deviation of the disturbed velocity from the undisturbed velocity will depend on the size of the particle relative to the computational grid, the grid geometry, the interpolation scheme and the particle Stokes and Reynolds numbers, as was shown by Horwitz & Mani (2016); Esmaily & Horwitz (2017). Therefore, a procedure for accurate computation of $\boldsymbol{u}_{\mathrm{f}}$ that correctly captures the influence of the particle on the fluid velocity field is required.

Based on our earlier work (Esmaily & Horwitz 2017), $\boldsymbol{u}_{\mathrm{f}}$ can be estimated by subtracting the disturbance created by the particle from $\boldsymbol{u}_{\mathrm{d}}$ as

$$\boldsymbol{u}_{\mathrm{f}} = \boldsymbol{u}_{\mathrm{d}} - \boldsymbol{u}_{\mathrm{c}}, \tag{2.6}$$

in which $\boldsymbol{u}_{\mathrm{c}}$ is the disturbance velocity created by the particle at the location of the particle. In the discrete setting, it is the fluid velocity on the Eulerian grid created in response to the two-way coupling force $\boldsymbol{F}$. Thus, the disturbance velocity can be considered as the response of the Navier-Stokes equations to a force $\boldsymbol{F}$ that is applied to a volume that is similar in size to the computational cell. Provided that the flow within the computational cell does not vary spatially and is represented by the single velocity $\boldsymbol{u}_{\mathrm{c}}$, we model the computational cell as a solid object that has the dimension of the computational cell that is held in place by $\boldsymbol{F}$ in a cross flow with velocity $\boldsymbol{u}_{\mathrm{c}}$. For an isotropic grid with size a, that solid object would be a cube of size $a \times a \times a$. Therefore, to estimate $\boldsymbol{u}_{\mathrm{c}}$, we solve for the velocity of that small solid cube that is surrounded by the fluid and dragged by $\boldsymbol{F}$.

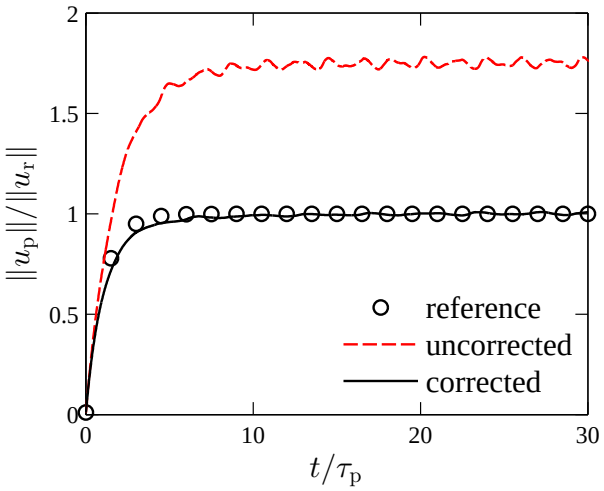

FIGURE 1. The settling velocity of a particle falling under gravity predicted by the two-way coupled point-particle simulation with (solid) and without correction (dashed). The circles are the reference analytical solution. Results correspond to a case in which the particle and the grid have the same size [adapted from Esmaily & Horwitz (2017)].

Since the computational cell is small and its Reynolds number is similar to that of the particle, we employ Eq. (2.1) to model its velocity. Since $\boldsymbol{u}_c$ is the deviation of the cell velocity from an undisturbed base flow, the undisturbed velocity of the computational cell itself is zero. Hence, its equation of the motion in direction i simplifies to

$$\frac{3}{2}m_c\dot{u}_c^{(i)} = -3\pi\mu d_c K_t^{(i)} u_c^{(i)} - F^{(i)}, \tag{2.7}$$

where $d_c = (6/\pi)^{1/3}a$ is the diameter of a sphere that has the same volume as the computational cell, $m_c = (\pi/6)\rho_f d_c^3 = \rho_f a^3$ is the mass of the computational cell defined earlier, and $K_t^{(i)}$ is the drag correction factor defined below. Note that the acceleration term is multiplied by 3/2 in Eq. (2.7) to account for the added mass.

The correction scheme employed in this study is governed by Eq. (2.7). This equation is integrated alongside Eq. (2.1) to obtain $\boldsymbol{u}_c$, which then is used to correct $\boldsymbol{u}_d$ via Eq. (2.6) to obtain the undisturbed velocity. Note that $\boldsymbol{u}_c$ is expressed in a Lagrangian frame that is attached to the particle. Thus, one $\boldsymbol{u}_c$ is computed for each particle. After substituting for $\boldsymbol{u}_f$ using Eq. (2.6), the corrected point-particle method is governed by six equations [Eqs. (2.1) and (2.7)] and six unknowns ($\boldsymbol{u}_p$ and $\boldsymbol{u}_c$), in contrast to the traditional point-particle approach, which assumes $\boldsymbol{u}_c = 0$ and is governed by three equations and unknowns (Eq. (2.1) and $\boldsymbol{u}_p$, respectively) per particle.

What remains is defining $K_t^{(i)}$, a correction factor to account for the deviation from the Stokes drag. Equation (2.7) without $K_t^{(i)}$ governs the motion of one spherical object subjected to a single force that is stationary in space. However, since the computational cell is a cube, the force is not always applied to one computational cell for a higher-order interpolation scheme, and the force moves with the particle throughout the grid. These additional effects are captured by

$$K_t^{(i)} = \frac{K_c C_r}{K_p^{(i)} C_t^{(i)}}. \tag{2.8}$$

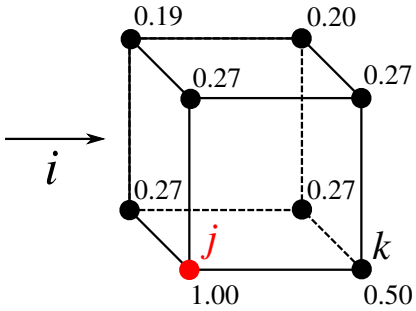

FIGURE 2. Value of $\alpha_{jk}^{(i)}$ for an isotropic grid, defined with respect to the direction i, where j is the computational cell at the anterior bottom left corner and k is a computational cell at one of the other corners. For instance, if k denotes an adjacent computational cell, that relative to j, is positioned perpendicular to i, then $\alpha_{jk}^{(i)} = 0.27$.

K_c accounts for the non-sphericity of the computational cell and is 0.516 for cube-shaped computational cells, i.e., isotropic grids. This value for K_c originates from an adjusted empirical relationship for the drag on prisms at low Reynolds numbers (Leith 1987). C_r accounts for the finite Reynolds number effect and is computed using the same empirical equation as the particles (Eq. (2.3)) using the computational cell Reynolds number $\|\boldsymbol{u}_\mathrm{c}\| d_\mathrm{c}/\nu$ instead. $K_\mathrm{p}^{(i)}$ accounts for the distribution of $\boldsymbol{F}$ among multiple computational cells and is computed as

$$K_\mathrm{p}^{(i)} = \beta_j^{(i)} \alpha_{jk}^{(i)} \beta_k^{(i)}, \tag{2.9}$$

where $\beta_j^{(i)}$, which depends on the location of particle in the computational cell, is the interpolation factor relating the fluid velocity at the location of particle to an adjacent computational cell j in direction i. The same interpolation factors are employed for the distribution of $\boldsymbol{F}$ to the adjacent computational cells, hence the symmetric form of Eq. (2.9). $\alpha_{jk}^{(i)}$ in Eq. (2.9) is the disturbance induced at the computational cell j in direction i relative to the disturbance created by $\boldsymbol{F}$ at the computational cell k in direction i (or vice versa). It is computed analytically in general on the basis of the velocity field around a sphere at low Reynolds numbers (Esmaily & Horwitz 2017). For an isotropic grid, it reduces to five numbers as far as adjacent computational cells are concerned, which would be the case for trilinear and low-order interpolation schemes. These numbers depend on the relative position of j and k with respect to the direction i. For instance, if j and k are aligned with direction i, $\alpha_{jk}^{(i)} = 0.50$, and if they are the same, $\alpha_{jk}^{(i)} = 1.00$ (Figure 2).

Lastly, $C_\mathrm{t}^{(i)}$ accounts for the limited exposure of a particle to a computational cell and is computed as

$$C_\mathrm{t}^{(i)} = 1 - \frac{1}{\xi^{(i)}} \left(1 - \exp\left(-\xi^{(i)}\right)\right), \tag{2.10}$$

where

$$\xi^{(i)} = \frac{12 \nu a K_\mathrm{c}}{d_\mathrm{c}^2 |u_\mathrm{p}^{(i)}|} \tag{2.11}$$

is the typical time for a particle to pass through a computational cell normalized by the computational cell relaxation time. Asymptotically, for a fast particle $\xi^{(i)} \to 0$, $C_\mathrm{t}^{(i)} \to \xi^{(i)}/2$, and since $u_\mathrm{c}^{(i)} \propto C_\mathrm{t}^{(i)}$, $\boldsymbol{u}_\mathrm{c} \to 0$. That is a limit that renders the need of having a correction scheme in the first place. By contrast, for a slow particle, $\xi^{(i)} \to \infty$

and $C_{\mathrm{t}}^{(i)} \to 1$, a limit at which particles can be assumed to be stationary on the grid, and no correction for the limited exposure would be needed.

3. Decaying particle-laden isotropic turbulence

In this section, we evaluate the importance of the correction scheme on particle collision statistics in a decaying isotropic turbulence. We provide an overview of the simulations setup and the post-processing procedure before presenting the results and their implications.

We consider a decaying homogeneous isotropic turbulence laden with inertial particles at conditions matching a particle-resolved simulation reported by Subramaniam *et al.* (2014). In this study, we use the same setup except for using a larger number of particles to augment particle-particle collisions. From the two simulations reported by Subramaniam *et al.* (2014), we consider the case at $\mathrm{Re}_\lambda = 27$, where Re_λ is the Reynolds number based on the Taylor micro-scale. For the sake of completeness, we briefly describe the conditions of that simulation and then compare the results of various modeling schemes.

An isotropic turbulent flow is generated on the basis of an energy spectrum that matches that of the particle-resolved simulation, which is obtained from Pope's model spectrum (Pope 2000), using Rogallo's procedure (Rogallo 1981). The diameter and density of the particle are selected such that at $t = 0$, $d_{\mathrm{p}} = \eta$ and $\mathrm{St} = 1$, where η is the Kolmogorov length scale and St is the particle Stokes number based on the Kolmogorov time scale. The domain is seeded with particles that are initially at rest. In contrast to Subramaniam *et al.* (2014) whose computations are performed at a mass fraction ratio of 1.8%, we increase the number of particles to obtain a mass fraction of one in this study. The computational domain is discretized on a 96^3 isotropic grid with $a = d_{\mathrm{p}}$. On the basis of the above parameters, the density ratio $\rho_{\mathrm{p}}/\rho_{\mathrm{f}} = 18$ and the volume fraction is 5.56%, which corresponding to $N_{\mathrm{p}} = 93873$ as the number of particles in the entire domain. Simulations are performed using an in-house code (Esmaily *et al.* 2015).

A hard-sphere collision model is adopted that is optimized with a cost that scales as $\mathcal{O}(N_{\mathrm{p}})$. All collisions are considered to be elastic with a coefficient of restitution of one. Since particles are randomly distributed in space at $t = 0$, there is a possibility of particle-particle overlapping in the initial seeding. To remove this artifact at the pre-processing step, we identify overlapping particles and separate them by a small distance. Since moving particles may lead to newly overlapping particles, this process is repeated until all particles are separated. This non-overlapping distribution of particles is employed for the initialization of all simulations. Additionally, since the hard-sphere collision model detects only binary collisions within a time step, some particle-particle collisions can go undetected, leading to overlapping particles as time passes. To minimize the number of overlapping particles, we use a very small time step size in our calculations ($\Delta t = 0.004\tau_\eta$, with τ_η being the Kolmogorov time-scale).

In total, we perform three sets of simulations. In the first approach, denoted no momentum coupling below, we neglect the effect of two-way coupling forces on the fluid momentum equation. In this case, the fluid velocity is not modified by the particles and decays freely owing to unladen dissipation. In the second approach, denoted uncorrected below, we incorporate the two-way coupling forces in the fluid momentum equation but use the disturbed velocity to compute the drag. In this case, which corresponds to a traditional four-way coupled simulation, $\boldsymbol{u}_{\mathrm{c}} = 0$ and $\boldsymbol{u}_{\mathrm{f}}$ in Eq. (2.1) is replaced by $\boldsymbol{u}_{\mathrm{d}}$. In the third approach, denoted corrected below, we account for two-way coupling forces

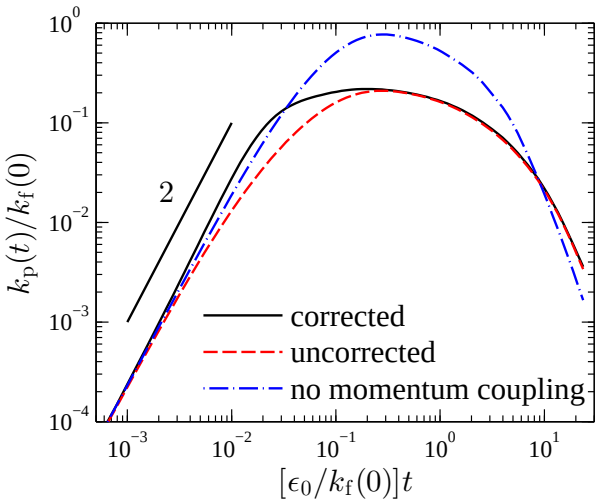

FIGURE 3. The kinetic energy of the particles in a decaying homogeneous isotropic turbulence as a function of time, obtained from the point-particle simulations with no momentum coupling (dash-dotted), with momentum coupling that is uncorrected (dashed) and with momentum coupling that is corrected (solid). Computations are performed at a mass-loading ratio of 1 and $\mathrm{Re}_\lambda = 27$ on a grid that has the same size as the particles and the Kolmogorov length scale at $t = 0$.

and use the correction scheme given in Section 2 to estimate the undisturbed velocity. Particle-particle collisions are accounted for in all these simulations.

In what follows, we first compare the results of these simulations in terms of energetics and then compare collision and clustering statistics. The particle kinetic energy is computed as

$$k_\mathrm{p}(t) = \frac{1}{2N_\mathrm{p}} \sum_{i=1}^{N_\mathrm{p}} \|\boldsymbol{u}_{\mathrm{p},i}(t)\|^2, \tag{3.1}$$

where $\boldsymbol{u}_{\mathrm{p},i}(t)$ denotes the velocity of the i^{th} particle. As shown in Figure 3, k_p is zero at $t = 0$ since particles are initially at rest. As time passes, particles accelerate as they are dragged by the fluid, increasing k_p. At very long times, the energy is eventually dissipated by the fluid, reducing the kinetic energy of the particles. The peak value of k_p and the time at which it occurs show dependence on the numerical scheme. Consistent with our earlier observation (Esmaily & Horwitz 2017), taking the corrected simulation as the reference here, no momentum coupling produces a higher peak that is slightly time advanced, whereas the momentum coupling with no correction produces a lower peak that is time delayed. The uncoupled simulation is not energy conservative and neglects to subtract the energy that is transferred to the particles from the fluid. Not removing energy from the system is what causes the higher peak of k_p. By contrast, the uncorrected simulation underestimates the drag on the particles, leading to a lower rate of energy transfer between fluid and particles, which in turn predicts a lower peak for k_p. Our earlier work (Esmaily & Horwitz 2017) showed that the corrected point-particle model, in contrast to the two other schemes, agrees well with a particle-resolved simulation in predicting the rate of energy transfer and consequently the magnitude and timing of the peak.

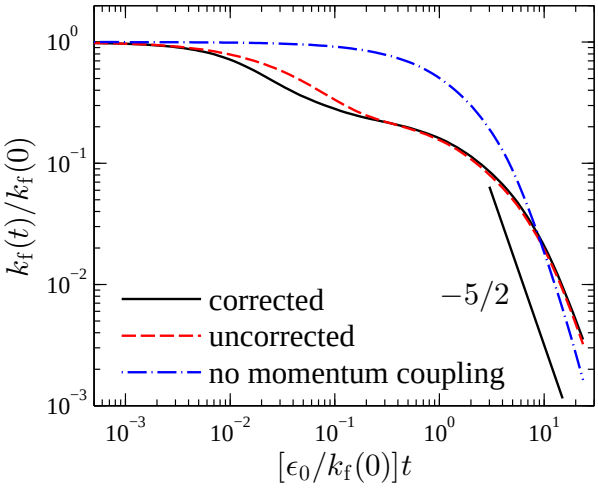

FIGURE 4. The kinetic energy of fluid in a particle-laden decaying homogeneous isotropic turbulence as a function of time. Refer to caption of Figure 3 for further details.

The fluid kinetic energy is computed as

$$k_\mathrm{f}(t) = \frac{1}{V}\int_V \frac{1}{2}\|\boldsymbol{u}(\boldsymbol{x},t)\|^2 \mathrm{d}V, \tag{3.2}$$

in which V is the volume occupied by the fluid in theory that is typically replaced by the volume of the entire computational domain in point-particle simulations. Utilizing this approximation in the governing equations of the fluid motion introduces an error in the order of particle volume fraction. Considering the relatively small volume fraction in our case study, we adopt this simplification to compute k_f (Figure 4). A monotonic decrease in k_f is observed, which is partly a result of the transfer of energy from the fluid to the particle at the early time and partly a result of its dissipation through viscous forces. The former mechanism is neglected in the simulation with no momentum coupling, producing the highest k_f for an extended period. The corrected simulation, however, produces the highest rate of energy transfer to the particles owing to its augmented drag prediction, thereby yielding the lowest k_f at the intermediate times.

At very short times, before the transfered energy is significant enough for the fluid or particle to change its velocity, k_f is fairly constant and k_p increases proportional to t^2 (Figures 3 and 4). This proportionality can be explained by the constant acceleration of particles, yielding $u_\mathrm{p} \propto t$ and consequently $k_\mathrm{p} \propto u_\mathrm{p}^2 \propto t^2$. What is remarkable, however, is that the corrected scheme predicts a faster-than-t^2 rate of increase of k_p for a brief period when it surpasses the value of k_p predicted by the simulation with no momentum coupling. This superlinear acceleration, which is also observed in the particle-resolved simulation results, can be attributed to the formation of a boundary layer around particles where fluid decelerates rapidly to adjust its velocity to that of the particle.

The kinetic energy of particles matches that of the fluid once the system reaches an equilibrium. At this point, the direction of transfer of energy reverses, with particles now transferring their energy to the fluid. The point of reversal coincides with the peak of k_p in each simulation, after which k_p becomes larger than k_f. For $t > 10k_\mathrm{f}(0)/\epsilon_0$, the kinetic energy of the case with no momentum coupling drops below the coupled simulations.

The same is also true for the rate of dissipation, computed as

$$\epsilon(t) = -\frac{\mathrm{d}}{\mathrm{d}t}\left[k_{\mathrm{f}}(t) + k_{\mathrm{p}}(t)\right], \tag{3.3}$$

which is higher for the coupled simulation at very long times† (Figure 5). The lower dissipation rate of the uncoupled simulation leading to a lower kinetic energy is a counterintuitive observation that can be explained by the lack of an energy transfer mechanism from the particles to the fluid. In this period, the inertial effects become negligible and $k_{\mathrm{f}} \propto t^{-5/2}$ for the uncoupled case, a result that is compatible with the theory of Batchelor & Townsend (1948) for the decaying unladen turbulence. Within the same period, the corrected and uncorrected schemes' predictions collapse in terms of k_{p}, k_{f} and ϵ. The explanation for this behavior lies in the behavior of $\epsilon(t)$ at early times, which varies such that the total dissipated energy at the equilibrium point is the roughly the same between the two simulations. Hence, the remaining kinetic energy of the system is similar between the two cases, producing the collapse in k_{p} and k_{f} plots. The collapse of the dissipation rate itself can be explained by the small slip velocity of the particles at the equilibrium that minimized the contribution of unresolved scales —modeled by the Stokes drag equation —on the total dissipation (Subramaniam *et al.* 2014).

How the dissipation rate behaves before the equilibrium point is unique to these simulations and was not clearly observed at lower loading (Esmaily & Horwitz 2017). The dissipation rate predicted by the corrected scheme is higher at short times, then drops below that of the uncorrected approach until they both converge at a very long time. This non-monotonic relative variation is a result of competition between the drag force and the slip velocity prediction by the two models, with the corrected scheme always predicting a higher and lower value for the former and latter, respectively. Thus, the product of the two, which is the dominant part of the dissipation rate at early times, can increase or decrease when the present correction is incorporated into the simulations.

As a side note, repeating these cases with no particle-particle collisions led to energetics that were indistinguishable from those presented here. Thus, we forgo presenting them here for the sake of brevity.

Next, we consider the collision frequency f_{c}, defined as the number of times a particle collides with surrounding particles in a time unit (i.e., $[\epsilon_0/k_{\mathrm{f}}(0)]t$). Figure 6 shows variation of f_{c} versus t. Since particles are stagnant at $t = 0$, only particles whose initial positions are very close collide. As particle accelerate, the number of collisions also rises in all cases. This trend continues even for $t > 0.3k_{\mathrm{f}}(0)/\epsilon_0$, when the particles' velocity decreases on average, according to Figure 3. This increase in the collision frequency suggests the formation of clusters at the longer time, in which there is a higher probability of finding particle pairs that are close enough to collide. This trend, however, is expected to reverse as particles come to rest at times beyond what is simulated here.

The collision frequency is significantly affected by the modeling approach. To further analyze this difference, we ensemble-averaged the relative velocity of particles at the time of the collision and normalized it by the average particle velocity (Figure 7). Similar to the collision frequency, models deviate the most in their prediction of the collision velocity at the intermediate time when particles are the fastest. The corrected scheme predicts the lowest relative velocity during this period, whereas the simulation with no momentum

† Note that the second term on the right-hand side of Eq. (3.3) is dropped for the simulation with no momentum coupling; otherwise, an unphysical negative dissipation rate would be obtained.

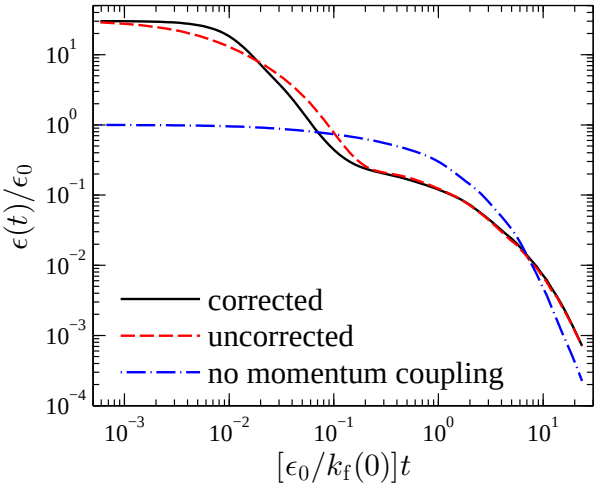

FIGURE 5. The rate of energy dissipation in a particle-laden decaying homogeneous isotropic turbulence as a function of time normalized by ϵ_0, which is the dissipation rate of the unladen flow at $t = 0$.

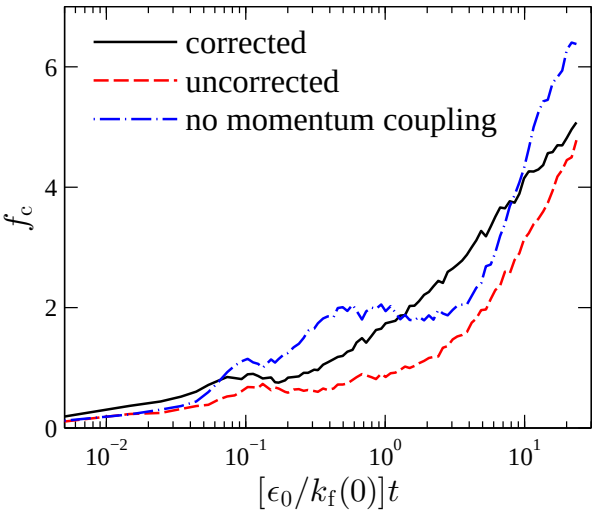

FIGURE 6. The collision frequency as a function of time for a particle-laden decaying homogeneous isotropic turbulence.

coupling predicts the highest. In summary, although the corrected scheme detects a larger number of collisions, most of them occur at a low relative velocity.

The above observation of the lower relative velocity of colliding particles is compatible with our earlier study, where we showed that the present correction scheme resolves the near-particle disturbances to a large extent (Esmaily & Horwitz 2017). We hypothesize that for two approaching particles in a stagnant flow, the disturbance in the velocity field acts as a repulsive mechanism that reduces the relative velocity of the colliding particles. The simulation without correction almost entirely fails to resolve this disturbance field,

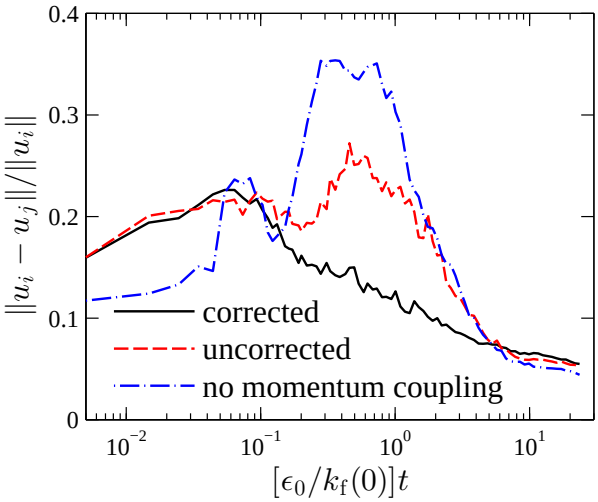

FIGURE 7. The ensemble average of the relative velocity of colliding particles normalized by the average particle velocity as a function of time.

thereby predicting a larger relative velocity of the colliding particle in comparison to the corrected scheme, which partly resolves that disturbance field. The substantial impact of the correction on these results underscores the need for a particle-resolved calculation that can truly resolve these disturbances and capture particle-particle interactions with higher accuracy.

Inertial particles in turbulent flows are known to preferentially concentrate in regions of high strain rate and low rotation rate (Maxey 1987; Squires & Eaton 1991; Eaton & Fessler 1994; Rani & Balachandar 2003; Esmaily & Mani 2016, 2017). The point-particle approach is commonly used in computational studies concerning preferential concentration. However, the adequacy of such models is uncertain, particularly in regimes of strong preferential concentration where the inter-particle distances can be very small. Earlier, we showed that the different point-particle schemes predicted large differences in particle radial relative velocity. This suggests that the transient configuration of particles may be different since particles will spend different residence times in the neighborhood of a partner. Hence, in what follows, we examine the degree of clustering predicted by each of the modeling approaches.

To quantify clustering, we employ

$$D_\mathrm{c}^2 = \frac{\sigma^2 - \lambda}{\lambda^2}, \tag{3.4}$$

where λ and σ are the mean and the standard deviation of the particle concentration field, defined on the fluid Eulerian grid with size a. The concept behind this formulation, which is discussed by Villafañe-Roca *et al.* (2016) in full detail, is to subtract λ from σ^2 to remove a bias associated with the Poisson randomness of particle positions on the grid, enabling one to obtain an estimate of the coefficient of variance of particle concentration field that is not sensitive to the number of particles.

For a random distribution of particles, D_c has an expected value of zero. For a fully uniform distribution of particles, where the inter-particle distances are the same in the entire domain, $D_\mathrm{c}^2 = -1$. In the present cases, where particles are randomly seeded

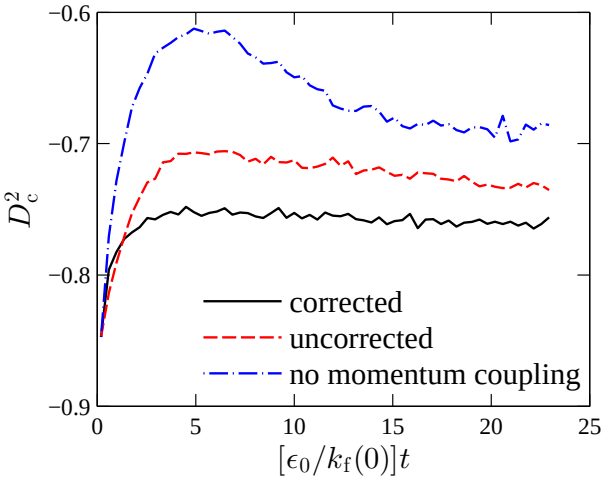

FIGURE 8. The clustering index for a decaying isotropic turbulence laden with particles that have St = 1 at $t = 0$. Various curves correspond to the different modeling strategies discussed in the caption of Figure 3.

and then displaced to eliminate particle-particle overlapping, D_c^2 has a value between -1 and 0 at $t = 0$ (Figure 8). As time passes, particles form clusters, creating a more intermittent concentration field with higher σ, which yields a larger D_c^2. After the initial transient period, however, D_c^2 decreases gradually since the Stokes number decreases to values smaller than one (owing to the turbulence decay), deviating from the regime of maximum preferential concentration that occurs at $\mathrm{St} = \mathcal{O}(1)$.

What is most intriguing in the results shown in Figure 8 is the strong dependence of D_c^2 on the modeling approach. The simulation with no momentum coupling predicts the strongest clustering, followed by the coupled simulation with no correction and the corrected coupled simulation, which predicts the lowest level of clustering. This trend is in accordance with our earlier hypothesis that resolving the near-particle disturbance repulses approaching particles, leading to a more uniform concentration field with a lower D_c^2. The corrected scheme yields the lowest D_c^2 since it is best at capturing those disturbances; followed by the uncorrected coupled scheme, which poorly captures those disturbances, yielding an slightly higher D_c^2; and finally the uncoupled simulation, which misses those disturbances completely, producing the highest D_c^2. The dependence of the clustering index on our modeling approach restates the importance of resolving the near-particle disturbances, warranting future studies to investigate this problem using particle-resolved simulations. These trends are specific to the regime under consideration and might reverse at a different volume fraction or Stokes number.

4. Conclusions

We have adopted a correction method for two-way coupled point-particle simulations that we originally proposed in Esmaily & Horwitz (2017). In that earlier study, we compared the results of our corrected point-particle method to those of a particle-resolved simulation performed by Subramaniam *et al.* (2014). We showed that the corrected scheme agrees remarkably well with the particle-resolved simulation in predicting particle and fluid energetics, whereas a conventional uncorrected scheme under-predicts the peak

of fluid dissipation and particle kinetic energy in particle-laden decaying homogenuous isotropic turbulence. We observed similar trends in this study, which was performed at a significantly higher mass-loading ratio. Provided that the volume fraction transport is not accounted for in our formulation, the accuracy of these results remains to be assessed by future particle-resolved simulations. Although no particle-resolved simulations were available for comparison, obtaining trends similar to those of the previous study suggests that the newly reported differences between corrected and uncorrected point-particle simulations may also be rooted in the inaccuracy of the uncorrected conventional point-particle model. Thus, the present study is a guide for identification of regimes and types of statistics that are most influenced by the missing scales in the point-particle simulations that ought to be resolved by higher-fidelity methods.

The need for a high-fidelity approach was demonstrated by considering particle-laden decaying homogeneous isotropic turbulence at a mass-loading ratio of one and a volume fraction of 5.5%. This case study represents a four-way coupling regime in which particle-particle interactions and momentum coupling are both critical. Apart from comparing energetics of the flow and particles that followed similar trends as the previous study (Esmaily & Horwitz 2017), we also examined the effect of momentum coupling and our correction scheme on the collision and clustering statistics. The sensitivity of those statistics to the modeling approach was remarkable. The collision velocity and the clustering index decreased and the collision frequency increased when two-way coupling forces were accounted for and even more when our correction scheme was employed. These trends were explained by the accuracy of each method in modeling the near-particle disturbances in the velocity field. Such disturbances are entirely absent in the uncoupled simulation, poorly captured by the uncorrected coupled simulation, and partly captured by the corrected scheme. Whether the degree to which these disturbances are resolved by our correction scheme is sufficient for accurate prediction of the statistics under consideration is a question that remains to be addressed by particle-resolved simulations or well-controlled experiments.

Acknowledgments

This investigation was funded by the Advanced Simulation and Computing (ASC) program of the US Department of Energy's National Nuclear Security Administration via the PSAAP II Center at Stanford, Grant #DE-NA0002373. The second author acknowledges support from the National Science Foundation Graduate Research Fellowship under Grant #DGE-114747.

REFERENCES

Ardekani, A. & Rangel, R. 2006 Unsteady motion of two solid spheres in Stokes flow. *Phys. Fluids* **18**, 103306.

Batchelor, G. 1972 Sedimentation in a dilute dispersion of spheres. *J. Fluid Mech.* **52**, 245–268.

Batchelor, G. & Townsend, A. 1948 Decay of isotropic turbulence in the initial period. *Proc. Roy. Soc. A*, **193**, 539–558.

Clift, R., Grace, J. & Weber, M. 2005 *Bubbles, Drops, and Particles*. Dover.

Eaton, J. & Fessler, J. 1994 Preferential concentration of particles by turbulence. *Int J. Multiphase Flow* **20**, 169–209.

Esmaily, M. & Horwitz, J. 2017 A correction scheme for two-way coupled point-particle simulations on anisotropic grids. In arXiv preprint, arXiv:1711.08084.

Esmaily, M., Jofre, L., Iaccarino, G. & Mani, A. 2015 A scalable geometric multigrid method for non-symmetric linear systems arising from elliptic equations. *Annual Research Briefs*, Center for Turbulence Research, Stanford University, pp. 211–223.

Esmaily, M. & Mani, A. 2016 Analysis of the clustering of inertial particles in turbulent flows. *Phys. Rev. Fluids* **1**, 084202.

Esmaily, M. & Mani, A. 2017 A modal analysis of segregation of inertial particles in turbulence. In arXiv preprint, arXiv:1704.00370.

Horwitz, J. & Mani, A. 2016 Accurate calculation of stokes drag for point–particle tracking in two-way coupled flows. *J. Comput. Phys.* **318**, 85–109.

Ireland, P. & Desjardins, O. 2017 Improving particle drag predictions in Euler-Lagrange simulations with two-way coupling. *J. Comput. Phys.* **338**, 405–430.

Leith, D. 1987 Drag on nonspherical objects. *Aerosol. Sci. Tech.* **6**, 153–161.

Maxey, M. 1987 The gravitational settling of aerosol particles in homogeneous turbulence and random flow fields. *J. Fluid Mech.* **174**, 441–465.

Pope, S. 2000 *Turbulent Flows*. Cambridge University Press.

Rani, S. & Balachandar, S. 2003 Evaluation of the equilibrium Eulerian approach for the evolution of particle concentration in isotropic turbulence. *Int. J. Multiphase Flow* **29**, 1793–1816.

Rogallo, R. 1981 *Numerical experiments in homogeneous turbulence*. NASA Tech. Memo. B1315.

Squires, K. D. & Eaton, J. K. 1991 Preferential concentration of particles by turbulence. *Phys. Fluids* **3**, 1169–1178.

Stimson, M. & Jeffrey, G. 1926 The motion of two spheres in a viscous fluid. *Proc. Roy. Soc. A* **111**, 110–116.

Subramaniam, S., Mehrabadi, M., Horwitz, J. & Mani, A. 2014 Developing improved Lagrangian point particle models of gas-solid flow from particle-resolved direct numerical simulation. *Proceedings of the Summer Program*, Center for Turbulence Research, Stanford University, pp. 5–14.

Sundaram, S. & Collins, L. 1997 Collision statistics in an isotropic particle-laden turbulent suspension. Part 1. Direct numerical simulations. *J. Fluid Mech.* **335**, 75–109.

Sundararajakumar, R. & Koch, D. L. 1996 Non-continuum lubrication flows between particles colliding in a gas. *J. Fluid Mech.* **313**, 283–308.

Villafañe-Roca, L., Esmaily, M., Banko, A. & Eaton, J. 2016 A robust method for quantification of preferential concentration from finite number of particles. *Annual Research Briefs*, Center for Turbulence Research, Stanford University, pp. 123–135.